Bulletin of Earthquake Engineering (2025) 23:6801–6828
https://doi.org/10.1007/s10518-025-02286-8

ORIGINAL ARTICLE

Seismic performance and fragility assessment of masonry infilled RC frames using a numerical approach

Saif Shaheen Kamil[1,2] · **Abu Bakar Nabilah**[1] · **Izian Abd. Karim**[1] · **Aidi Hizami Alias**[1] · **Mohd Zahirasri Mohd Tohir**[1]

Received: 18 April 2025 / Accepted: 12 September 2025 / Published online: 8 October 2025

Abstract
Damage to masonry infill walls can result in substantial property loss and pose a serious risk to human safety. The behaviour of masonry walls under seismic load and the corresponding consequences must be effectively characterized for reliable damage estimation. Some drift-based fragility functions have been proposed based on experimental datasets in literature; however, the high dispersion and inconsistencies of findings hinder their reliability in damage assessment. Therefore, this paper aims to derive a reliable fragility curve for reinforced concrete infilled frames using numerical analysis. The analysis models were designed based on different infill parameters, including type of panel, infill strength, wall thickness, and aspect ratio. The cracking and crushing of concrete and masonry were simulated using the total strain crack model. The findings were validated against several experimental studies in the literature. A new damage state definition based on visible cracks ratio was proposed. The results indicate that damage capacity, crack pattern, and failure mode are strongly related to wall properties. It was also observed that infill strength and the presence of opening have a significant influence on the fragility of masonry infill.

Keywords Masonry infills · In-plane behaviour · Finite element method · Fragility curves

1 Introduction

Among natural hazards, earthquakes are one of the most devastating natural events due to their catastrophic influence on civil structures in terms of loss of functionality, social consequences, monetary losses, and casualties (Erdik et al. 2023; d'Aragona et al. 2024).

✉ Abu Bakar Nabilah
nabilah@upm.edu.my

Saif Shaheen Kamil
saifshaheen93@gmail.com

[1] Faculty of Engineering, Universiti Putra Malaysia, Serdang, Selangor 43400, Malaysia

[2] Department of Civil Engineering, College of Engineering, Al-Nahrain University, Baghdad, Iraq

The damage analysis has highlighted the significant impact of non-structural components on earthquake damage, however, infill panels are generally neglected in practice-oriented structural analyses for design or assessment purposes (Demirel et al. 2023). Masonry infill walls are stiff but have relatively low strength compared to the surrounding frames, making them susceptible to significant damage at low lateral drifts when the system is elastic (Furtado et al. 2020; Dias-Oliveira et al. 2022).

The recent regulations of seismic performance assessment methodologies have emphasized the necessity of correlating building damage states with engineering demand parameters to establish a robust component fragility curve (Banihashemi et al. 2024). Subsequently, building component damage states are transformed into performance evaluation metrics using a defined loss function.

Damage states (DSs) for masonry infill have been proposed by some seismic codes. In most cases, designers are required to check the specified limit for inter-story drift (ISD) irrespective of the infill walls varying material and geometric properties. FEMA 356 (2000) developed three performance levels, namely immediate occupancy, life safety, and collapse prevention corresponding to specific ISD limits, while Eurocode 8 (2005) set a limit between 0.5% and 1% for infill RC frames and a drift ratio within 1/50 was recommended by GB 50011−2010 (2016). However, most codes lack specific provisions for limiting in-plane damage to infill walls, as the influence of infill material properties on the damage limits is often not considered.

Although there has been extensive research on masonry infill walls, the majority of studies have mainly concentrated on improving the understanding of their seismic response through the evaluation of strength and stiffness. Some researchers, utilizing infill wall experimental databases, have associated in-plane drift limits of infill walls with different DSs. Cardone and Perrone (2015) developed drift-based fragility functions using 55 specimens from 19 studies. Sassun et al. (2016) also established a set of in-plane fragility functions using experimental data. The results highlighted the significant impact of wall properties, such as unit type, on the fragility functions. Chiozzi and Miranda (2017), on the other hand, indicated that unit type has no significant effect on all damage states, which is the opposite of the findings reported by Sassun et al. (2016). Risi et al. (2018) derived in-plane fragility functions for masonry infill with hollow clay brick. The researchers reported a significant effect of masonry compressive strength and unit hole direction for DS2 and DS4. However, only two damage states were estimated for panels with openings due to limited data about damage progress. Xie et al. (2022) investigated the influence of brick and wall typology on in-plane fragility function by conducting an experimental test on nine full-scale infill RC frames. The researchers highlighted that the type of brick did not have an important effect on all DSs. Liu et al. (2022) collected data from 46 studies to develop in-plane fragility functions with four damage states. The proposed fragility function shows high dispersions for all damage states ($\beta > 0.6$) which exceed the FEMA P-58 (2018) limitation for high-quality fragility curves. Liu et al. (2024) derived fragility functions based on comprehensive experimental data considering the effect of material properties, geometric features, and in-plane and out-of-plane load interactions. It was found that the compressive strength of masonry infill is the major influencing factor across all DSs, while a limited impact of slenderness ratio (SR) and aspect ratio (AR) was reported.

The majority of the adopted experimental data for the development of fragility function (Cardone and Perrone 2015; Sassun et al. 2016; Chiozzi and Miranda 2017; Risi et al. 2018;

Liu et al. 2022, 2024) were conducted on RC frame (84%), aspect ratio (h_i/l_i) less than 1.0 (75%), wall thickness (t_i) of less than 150 mm (80%), and masonry strength (F_m) of less than 8 MPa (75%) as summarized in Fig. 1. While these characteristics reflect typical configurations in experimental studies on infill walls, tests on RC frames with high-strength infills, thicker walls, a wider range of aspect ratios, and openings remain limited in the current database. In this context, several experimental studies have demonstrated that aspect ratio, material type, wall thickness, and the presence of openings are among the most influential parameters governing the in-plane seismic behaviour of masonry infill walls (Mehrabi et al. 1996; Calvi and Bolognini 2001; Al-Chaar et al. 2002; Cavaleri et al. 2005; Stylianidis 2012; Hak et al. 2013, 2017; Kubalski et al. 2017; Morandi et al. 2018, 2025; Butenweg et al. 2019). Diagonal compression failure typically occurs in slender walls (h_i/l_i >1.5), while sliding shear and corner crushing failure are primarily observed in squat walls ($h_i/l_i \leq 1$) (Asteris et al. 2011; Basha and Kaushik 2016). Material properties also significantly influence the behavior of masonry infill. Hollow brick showed a higher drift capacity than solid brick at a high damage state (Del Gaudio et al. 2019), and strong infill provided greater strength, stiffness, and energy dissipation under seismic loading compared to weak infill (Kakaletsis and Karayannis 2008; Furtado and de Risi 2020). Thick infill walls enhance in-plane strength and damage resistance under seismic loading by improving brick interconnection and limiting perpendicular joint vulnerability (Huang et al. 2012; da Porto et al. 2013; Misir et al. 2016). Openings generally reduce lateral strength, stiffness, and energy dissipation, with the

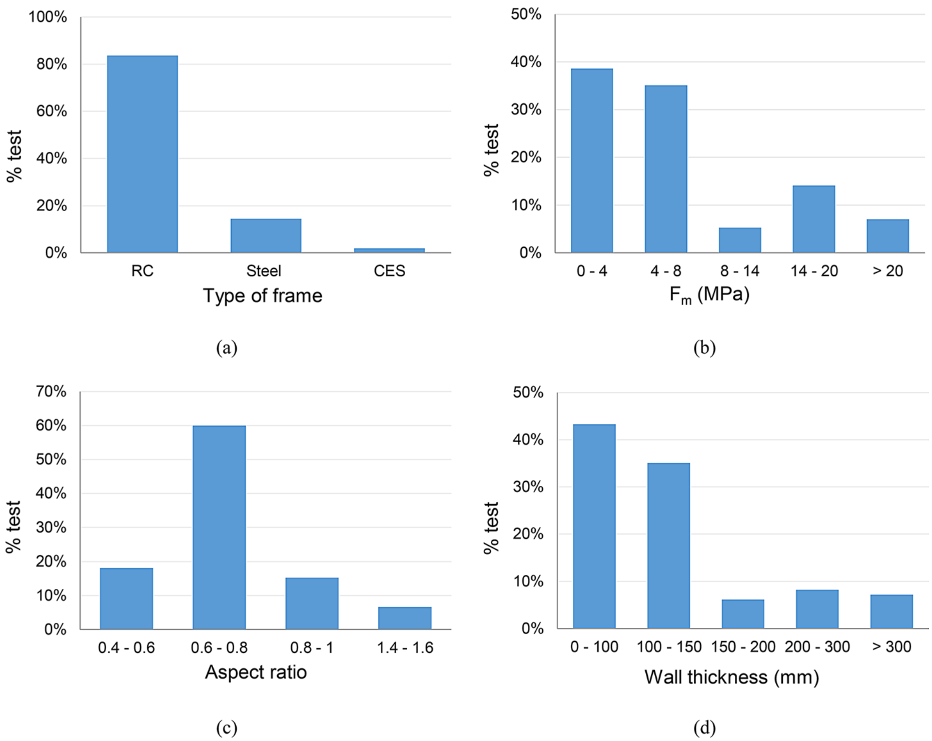

Fig. 1 Infill properties distribution for the collected database of 100 specimens based on (**a**) type of frame, (**b**) masonry strength (F_m), (**c**) aspect ratio, and (**d**) wall thickness

extent of reduction depending on opening size and void ratio (Combescure and Pegon 2000; Sigmund and Penava 2012; Decanini et al. 2014; De Risi et al. 2018). Failure modes also influence drift capacity, with sliding shear failures allowing higher drifts before collapse. Even after cracking or sliding, infill panels maintain some lateral strength capacity for the infilled frame (Dias-Oliveira et al. 2022).

While geometry, material properties, wall thickness, and openings are recognized as key parameters influencing the seismic performance of infill walls, there remains a lack of consensus regarding their specific effects on in-plane capacity, failure mechanisms, and damage evolution (De Risi et al. 2018; Chiozzi and Miranda 2017; Shah et al. 2019). For instance, it is widely accepted that wall thickness can significantly impact the in-plane damage states of infill walls. However, Liu et al. (2024) reported that wall thickness does not affect in-plane drift beyond damage thresholds, indicating inconsistencies in the literature regarding the influence of wall thickness on in-plane behaviour. Similarly, Kakaletsis and Karayannis (2008) found that openings increase drift capacity, while other studies report significant reductions in in-plane capacity for infills with openings compared to solid panels (Xie et al. 2022; Di Trapani et al. 2024).

Although numerous variables have been identified in previous research regarding in-plane capacity and damage assessment, the conflicting findings and large variations undermine their reliability in evaluating the damage. Also, determining DSs from existing test results presents challenges due to inadequate descriptions of damage to masonry walls. The absence of quantitative damage data and reliable criteria for DS determination undermines the reliability of fragility functions and may contribute to contradictory research findings. To overcome these limitations, a comprehensive investigation of infill walls with diverse characteristics, particularly in terms of damaged behaviour, is essential. Experimental tests incur high costs and are time-consuming, while the contribution of infill to overall frame response should be considered. Consequently, numerical modelling is widely employed to accurately capture nonlinear phenomena and various crack patterns that develop at the masonry unit and joint levels (D'Altri et al. 2019; Iannacone et al. 2021).

This research seeks to address the key challenges in determining the probability of damage to masonry infill. It focuses on three critical aspects, namely characterizing infill material properties and their impact on the damage behaviour of infilled RC frames, assessing damage probability through multiple structures with a concentration on the interaction of the damage state with wall properties and applied load, and developing an effective method for damage quantification of infill walls. To this end, thirty-seven infill masonry walls with various parameters were analyzed using a micro finite element model. The influence of masonry infill compressive strength, aspect ratio, wall thickness, and the presence of openings have been meticulously assessed. A new definition of damage states concerning visible cracks was proposed. Drift-based fragility functions for masonry infill walls subjected to in-plane loading have been presented.

2 Numerical model

2.1 Model description

Several framed masonry specimens were designed at a scale of 2/3 to represent a single span of a typical multi-story residential building. The scaled specimens effectively capture key seismic performance parameters, such as drift capacity, cracking patterns, and stiffness degradation, as demonstrated in previous studies (Penava et al. 2016; Trapani et al. 2024), while reducing computational cost and providing consistency with available experimental data. Frames were designed as medium-ductility class (DCM) in compliance with Eurocode 8 (2005). The RC columns were fixed to a foundation beam of 400 × 400 mm cross-section. The longitudinal and transverse reinforcements with diameters of 12 mm and 6 mm respectively were designed for both columns and beams. The dimensions and reinforcements of the RC frames were identical for all the specimens and are shown in Fig. 2.

37 specimens with varying parameters, ranging from opening type, aspect ratio (AR), wall thickness, and infill strengths were developed, as shown in Table 1. The infilled RC frames were divided into two main categories, namely full infill wall (FI) and infill with opening. Depending on the type and location of the opening, the infilled frames were denoted as CW (centre window), SW (side window), and DO (middle door opening), as illustrated in Fig. 2 and identified by the first two letters in the specimen ID (Table 1). The opening percentages (A_o/A) were 16% and 22% for window and door openings respectively. The opening eccentricity (l_l/l_i), the ratio between the horizontal distance of the centre of the opening and the length of the infill, for the side window was equal to 0.3. Next, the walls were categorized based on the aspect ratio (h_i/l_i) of 0.6, 1, and 1.6. This is denoted by the middle number in the specimen ID. The height of the panel was kept constant at 2 m, except for specimens with an AR of 1.6, where a 3 m wall height was adopted. In each category, several wall panels were designed with thicknesses (t_i) of 10 cm and 20 cm, and low to high infill strength (F_m). The compressive strength of low-strength infill was 2 MPa mortar joint and 2 to 6 MPa brick units. On the other hand, high-strength infill was designed with 8 MPa mortar and brick strength between 12 and 18 MPa. The last number of the specimen ID refers to the strength and thickness of the infill, where L and H denote low and high strengths respectively, while 1 and 2 refer to 10 cm and 20 cm thickness respectively.

2.2 Material constitutive model

In this study, a simplified two-dimensional (2D) micromodel was adopted for analysis of the infill RC frame as only in-plane loading was applied. Mortar layers and the interfaces were concentrated in a zero-thickness interface, and masonry units were expanded to guarantee that the geometrical dimensions of the whole system remained the same. In this way, it was possible to capture the sequenced failure of the masonry infill wall and avoid modelling the mortar (Fig. 3). For each material, the appropriate constitutive law capable of describing its structural behaviour was used. The behaviour of concrete was described using the Maekawa-Fukuura model (Prionas et al. 2020). In this model, the compressive regime is depicted using a multi-axial damage plasticity model, and the tensile regime is expressed through a crack model based on total strain, along with a description of hysteresis in tensile

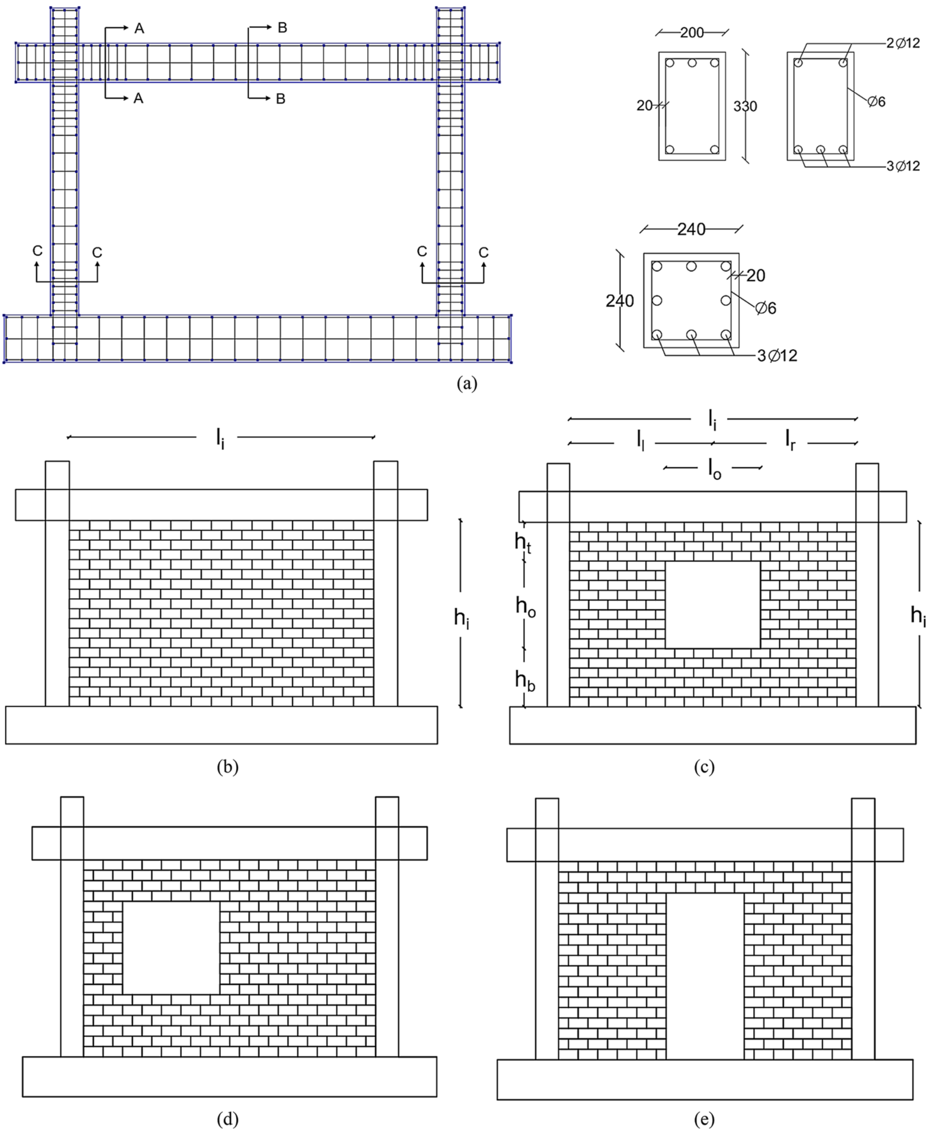

Fig. 2 Dimensions of analysed models, showing (**a**) detailing of RC frame, (**b**) full infill frame (FI), (**c**) central window opening (CW), (**d**) side window opening (SW), and (**e**) door opening (DO)

and compressive unloading-reloading loops. The concrete model input data is presented in Table 2.

The behaviour of masonry units was described using a total strain crack model with a rotated crack. It is based on a smeared failure approach for the fracture energy in which one stress-strain relation is used to describe the material behaviour in tension and compression (Ferreira 2021). The average value of Poisson's ratio for masonry is within the range of 0.13 to 0.15. The modulus of elasticity (E) of masonry can be evaluated using Eq. (1).

Table 1 Typological and geometrical features of the analysis models

Specimen ID	N^{a}	h_i (cm)	l_i (cm)	t_i (cm)	(h_i/l_i)	F_m (MPa)	l_o/h_o (cm)	A_o/A (%)	l_l / l_i
FI-0.6-L1	3	200	300	10	0.6	2–6	0	0	0
FI-0.6-L2	2	200	300	20	0.6	2–6	0	0	0
FI-0.6-H1	3	200	300	10	0.6	12–18	0	0	0
FI-0.6- H2	2	200	300	20	0.6	12–18	0	0	0
FI-1.0-L1	3	200	200	10	1	2–6	0	0	0
FI-1.0-L2	2	200	200	20	1	2–6	0	0	0
FI-1.0- H1	3	200	200	10	1	12–18	0	0	0
FI-1.0- H2	2	200	200	20	1	12–18	0	0	0
FI-1.6- L1	2	300	200	10	1.6	2–6	0	0	0
FI-1.6- H1	3	300	200	10	1.6	12–18	0	0	0
CW-0.6-L1	1	200	300	10	0.6	5	100/95	16%	0.5
CW-1.0-L1	1	200	200	10	1	5	90/70	16%	0.5
CW-1.6-L1	1	300	200	10	1.6	5	100/95	16%	0.5
CW-0.6-H1	1	200	300	10	0.6	12	100/95	16%	0.5
CW-1.0-H1	1	200	200	10	1	12	90/70	16%	0.5
CW-1.6-H1	1	300	200	10	1.6	12	100/95	16%	0.5
SW-0.6-L1	1	200	300	10	0.6	5	100/95	16%	0.3
SW-0.6-H1	1	200	300	10	0.6	12	100/95	16%	0.3
DO-0.6-L1	1	200	300	10	0.6	5	80/165	22%	0.5
DO-1.0-L1	1	200	200	10	1	5	70/130	22%	0.5
DO-0.6-H1	1	200	300	10	0.6	12	80/165	22%	0.5
DO-1.0-H1	1	200	200	10	1	12	70/130	22%	0.5

a N=number of analyzed specimens

$$E = a \cdot (Fm)^{b} \tag{1}$$

There is a significant variation in the coefficients *a* and *b* have been reported, where coefficient *a* ranges between 400 and 2500 and the coefficient *b* between 0.5 and 1 (Brooks 2015; Guadagnuolo et al. 2020). The average value for coefficients *a* and *b* was 328 and 1 as reported by Drougkas et al. (2015), which was adopted in this study. The Mode-I fracture energy (GF_I) of a masonry unit is considered to be 10% of its tensile strength (Baietti 2021), while Mode-II fracture energy (GF_{II}) is assumed to be 10 times GF_I (De Villiers 2019; Baietti 2021). The masonry model input parameters are given in Table 2.

The Mohr-Coulomb criterion with tension cut-off was selected to describe the contact between the masonry units as well as the infill and surrounding frame. For simplification purposes, the contact between masonry units, column and infill, and beam and the infill have been assumed to be the same. Initial elastic (K_{nn}) and shear stiffnesses (K_{tt}) were evaluated using the expressions from K_{nn} = E/t and K_{tt} = G/t, where E is the modulus of elasticity, G is shear of the surrounding material and t is the thickness of the mortar (Penava et al. 2019). Friction angle (Fa) in the range between 0 and 0.005 was adopted and cohesion (C_o) can be assumed equal to tensile strength (Milani and Lourenço 2013; Pluijm et al. 2000). The input data of bed and head joints are presented in Table 3.

The Menegotto-Pinto model was utilized for longitudinal and transversal steel reinforcements (Penava et al. 2016). The Young's moduli for longitudinal and transverse reinforcements were assumed to be 200 GPa and 180 GPa respectively. Yield stresses were assumed to be equal to 420 MPa for longitudinal and transverse reinforcements. The constants a_1 to

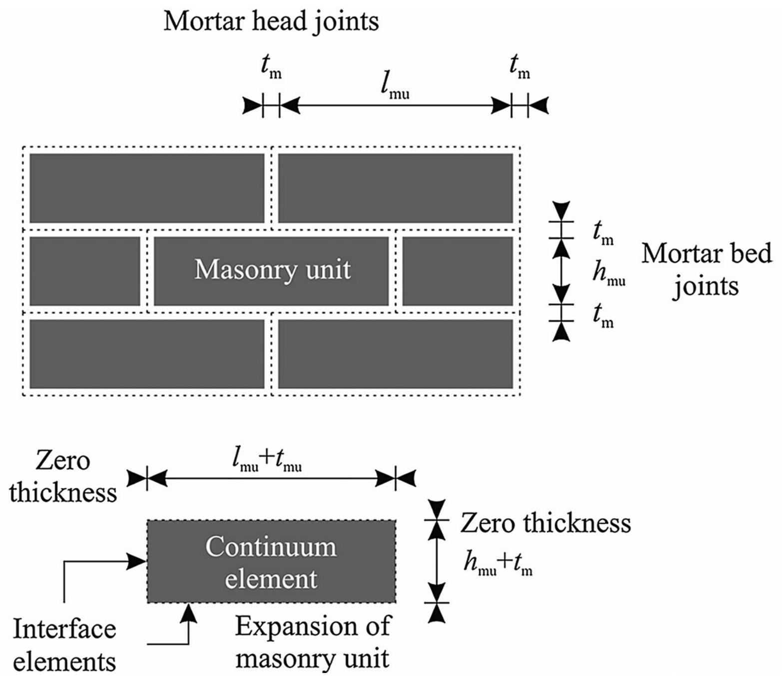

Fig. 3 Simplified micromodel (from Penava et al. 2016)

Table 2 Mechanical properties of concrete and brick units

Parameter	Concrete	Low-strength brick	High-strength brick
Young's modulus, Ex (MPa)	24,300	2100–4200	8400–11,900
Young's modulus, Ey (MPa)	-	1050–2800	1400–1750
Poisson's ratio, v (-)	0.16	0.13	0.13
Compressive strength, F_c (MPa)	27	3–6	12–17
Tensile Strength, F_t (MPa)	2.7	0.3–0.6	1.2–1.7
Mode-I tensile fracture energy, GF_I (N/mm)	-	0.015–0.03	0.06–0.085
Mode-II fracture energy, GF_{II} (N/mm)	-	0.15–0.3	0.6–0.85

Table 3 Mechanical properties of the interface

Parameter	Bed joint		Head joint	
	Low strength	High strength	Low strength	High strength
Compressive strength (MPa)	3	8	1.5	5
Young's modulus, E (MPa)	1750	5600	1050	3360
Shear modulus, G_X (MPa)	930–1860	3720–5260	470–1240	620–1300
Normal stiffness, K_{nn} (N/mm^3)	260–530	1050–1500	130–350	175–350
Shear stiffness, K_{tt} (N/mm^3)	120–250	660–750	60–160	80–160
Cohesion, C_O (MPa)	0.3	0.8	0.15	0.5
Friction angle, Fa (rad)	0.005	0.005	0.005	0.005
Dilatancy angle (rad)	0	0	0	0

a_4 are used for defining the hysteretic behaviour of the reinforcement, and they are evaluated based on the material's cyclic stress-strain response. The input parameters for reinforcement are shown in Table 4.

2.3 Element, mesh properties, and boundary conditions

Concrete and masonry units were modelled using quadrilateral isoperimetric plane finite elements with eight-node (CQ16M), reinforcement with a two-node bar element connected to the eight-node concrete element at the two external nodes, and a 3-point line interface element (CL121) for the interface. The adopted interface model is capable of modelling cohesion, separation, and cyclic behaviour. Mesh size significantly affects the quality of numerical results, where a fine mesh takes a long calculation time without significant improvements in accuracy, while a coarser mesh yields incorrect results. A mesh convergence study was performed by testing element sizes ranging from 1/2 to 1/10 of the structure element size, with 1/4 found to provide a good balance between accuracy and computational efficiency. Displacement and force boundary conditions were set similar to the experimental test conditions using a fixed-base beam and the prevention of vertical movement in the column ends. Vertical and lateral loads were applied at the beam-column joint and the beam ends respectively (Fig. 4). Vertical loads depend on force from upper stories, resulting in 10 to 16% of the column average capacity. In this study, a vertical load in the amount of 200 kN was applied to the top of the column, which simulates the loading from the upper floors. For proper load distribution, linear elastic steel pads were placed at the beam and column ends, as in the experimental tests. Newton–Raphson method was used to solve the non-linear equations.

2.4 Loading protocol

The selection of a loading protocol for unreinforced masonry walls should align with system properties and regional seismic demand, as displacement capacity is affected by the number of cycles to failure (Beyer et al. 2014). While standardised protocols developed for high-seismicity regions, such as ATC-24 (1992), often impose more cycles than necessary (Krawinkler 2009), the use of fewer cycles is recommended for testing masonry walls (Mergos and Beyer 2014). Reflecting these considerations, a unidirectional quasi-static cyclic loading protocol recommended by FEMA 461 (2007), appropriate for component-level fragility assessment under typical seismic demands, was utilised for developing fragility functions in this study. This load protocol can be used for structural and non-structural components (De Francesco et al. 2022). The quasi-static cyclic loading started from a drift amplitude of

Table 4 Mechanical properties of reinforcement

Parameter	Value
Young's modulus, E (GPa)	180
Yield stress, Fy (MPa)	420
Initial tangent slope ratio	0.0028
Initial curvature parameter	20
Constant a_1	18.5
Constant a_2	0.15
Constant a_3	0.01
Constant a_4	7

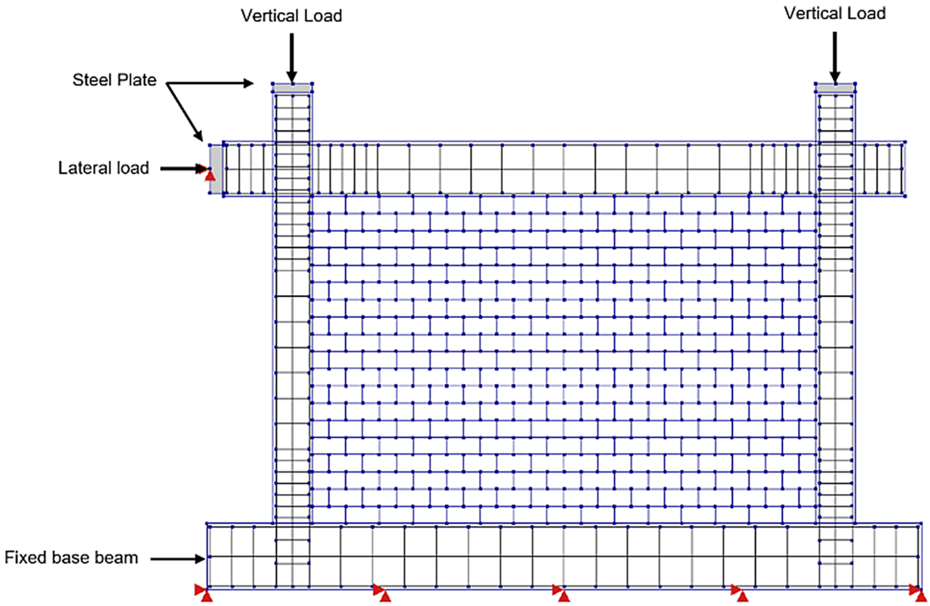

Fig. 4 Boundary condition of analysis models

1.5 mm. The amplitude was increased 1.4 times for each load increase with two repeated cycles for each amplitude to reach a maximum drift displacement of 84 mm.

3 Model validation

To validate the numerical findings, several experimental studies from literature with various infill properties were reproduced. The selected studies were conducted at different scales and included specimens with low brick strength solid infill (MV1) (Verderame et al. 2022), low bond strength solid infill (MV2) (refers to significantly weak tensile and shear bond at the unit-mortar interface), infill with window (MV3) and door (MV4) openings (Kakaletsis and Karayannis 2008), and high brick strength solid infill (MV5), and with openings (central window (MV6), side window (MV7), and door (MV8) (Trapani et al. 2024). These specimens provide detailed descriptions of damage progression and include variations in infill type and properties, aligning with the objectives of this study. While the use of scaled specimens may introduce some limitations, the unit dimensions in most validation specimens were configured to be compatible with the frame scale, either through unit scaling or by utilizing sufficiently small bricks to minimize scale effects on structural behavior (Kakaletsis and Karayannis 2008; Trapani et al. 2024). The primary purpose of the validation approach herein is to evaluate the validity of the numerical model in reproducing the experimentally observed damage mechanisms, crack patterns, and inter-story drift. The utilized models were able to reproduce the hysteresis loop of experimental specimens with high accuracy as reported in Fig. 5. The comparison between numerical analysis and the experimental results is presented in Fig. 6, which shows similar crack patterns and failure modes for all cases. Crushing of brick units with limited mortar sliding was observed

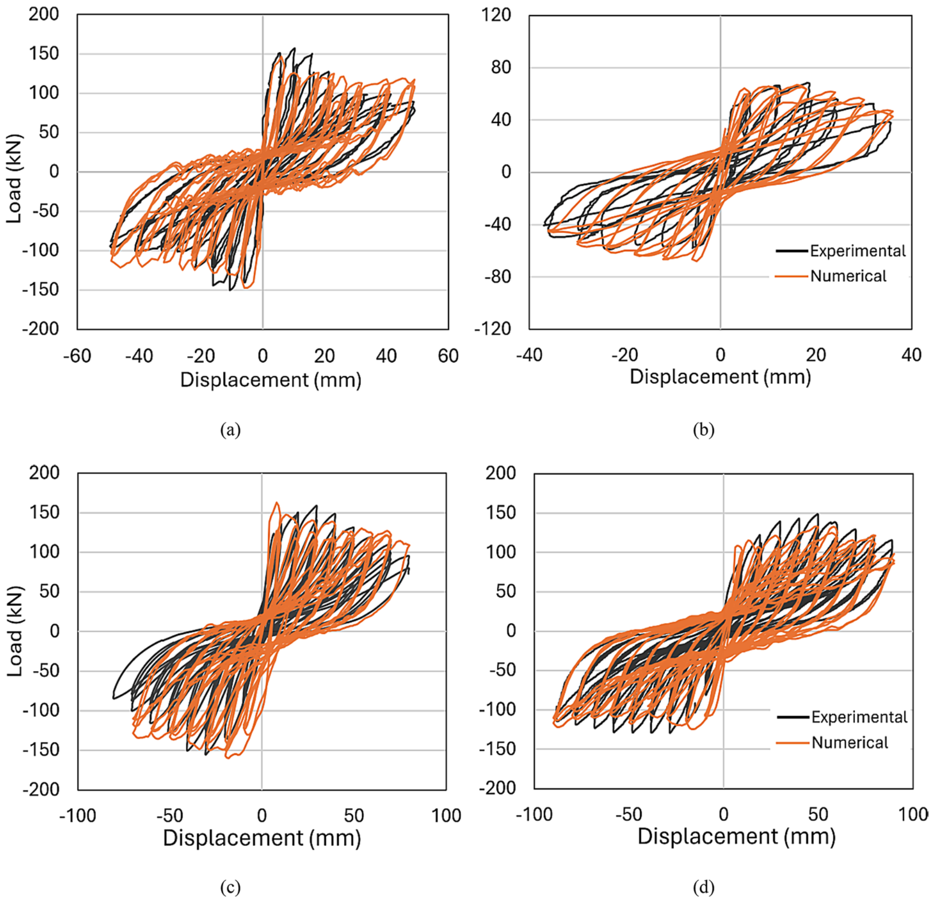

Fig. 5 Load-displacement curves for validation models (**a**) MV1 (solid), (**b**) MV3 (central window), (**c**) MV7 (side window), and (**d**) MV8 (door)

for MV1, which is designed with low-strength brick and high-strength mortar (Fig. 6(a)). Shear sliding of bed mortar with minor damage on bricks was the dominant failure mode for MV2 to MV4 with a low-strength mortar joint of 1.5 MPa (Fig. 6(b)). Intensive mortar sliding was noticed with lower damage on brick units for MV5 to MV8 (Fig. 6(c)). These were mainly related to the relative strength between brick and mortar, where damage was concentrated at the lowest strength compound. The crack width associated with the damage states (DS) of validation specimens has been also evaluated. Generally, the maximum crack width is 0.5 mm (DS1), 1 to 2 mm (DS2), and exceeds 2 mm (DS3 to DS4). Although the width of major cracks in some specimens was not reported experimentally (for example MV5 to MV8), reasonable results were found by numerical models, where cracks exceed 10 mm width at the collapse stage.

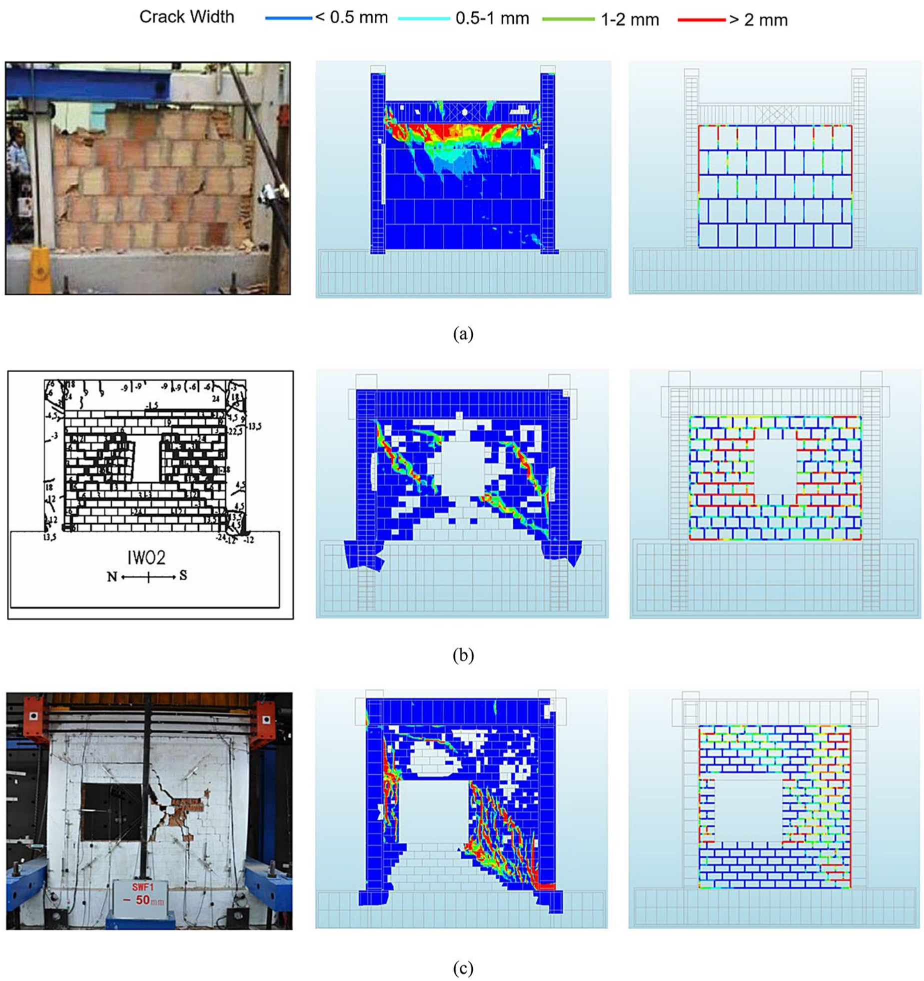

Fig. 6 Comparison between numerical and experimental crack patterns for (**a**) MV1 (Verderame et al. 2022), (**b**) MV3 (Kakaletsis and Karayannis 2008), and (**c**) MV7 (Trapani et al. 2024)

4 Results and discussions

4.1 Load displacement curves

Load displacement curves for the main analysis namely bare frame, short infill (AR = 0.6), square infill (AR = 1.0), and infill with opening are presented in Fig. 7, while the envelop curves are shown in Fig. 8 with varying infill strength and thickness. For all specimens, the maximum lateral load capacity of infilled frames was higher than the bare frames by approximately 2 times for low-strength infill (Fig. 7(b)) and 5 times for high-strength infill (Fig. 7(d) and 7(g)), while it is reduced to 1.75 to 2.75 times for low and high strength infill with openings respectively (Fig. 7(h) to 7(j)). The lateral resistance of high-strength infill was 1.6 times greater than the ones corresponding to low-strength solid panels. The effect of

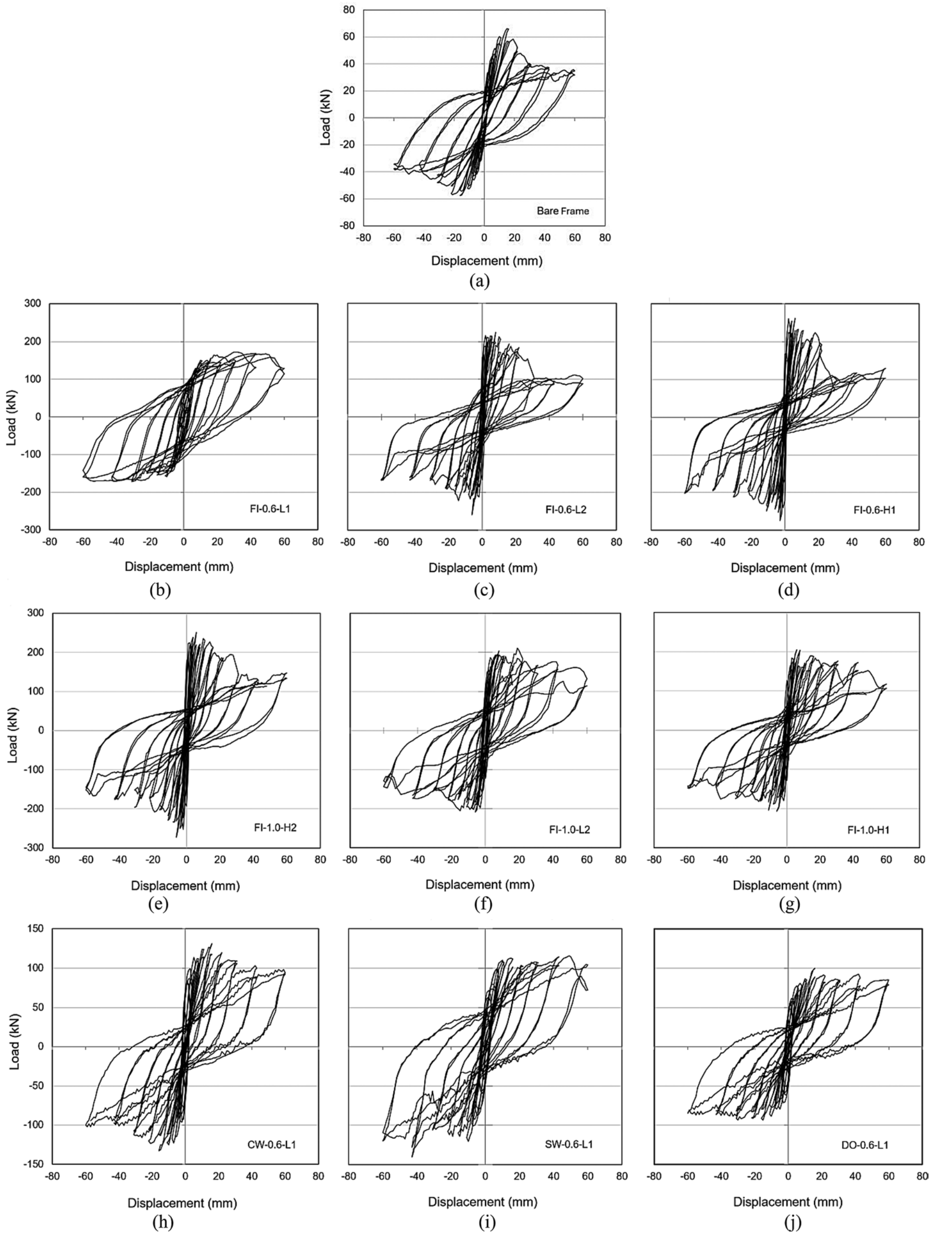

Fig. 7 Load displacement curves for samples; (**a**) bare frame, (**b**) FI-0.6-L1, (**c**) FI-0.6-L2, (**d**) FI-0.6-H1, (**e**) FI-1.0-H2, (**f**) FI-1.0-L2, (**g**) FI-1.0-H1, (**h**) CW-0.6-L1, (**i**) SW-0.6-L1, and (**j**) DO-0.6- L1

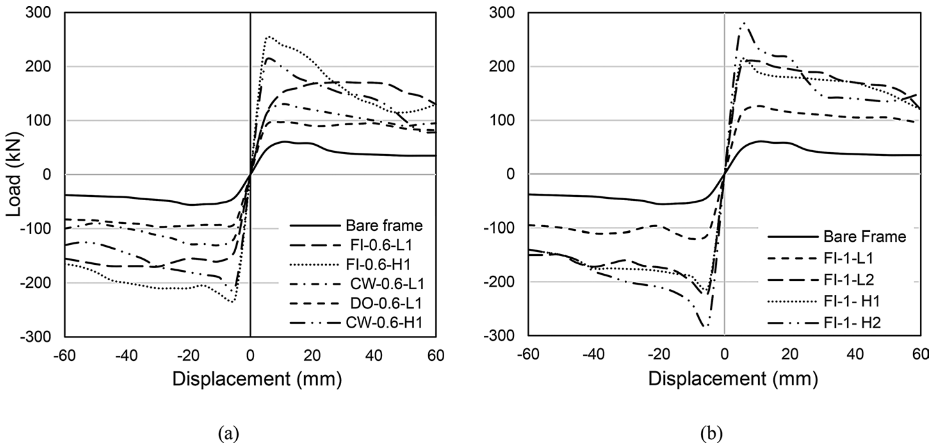

Fig. 8 Envelope curves from the analysis with varying infill (**a**) strength and (**b**) thickness

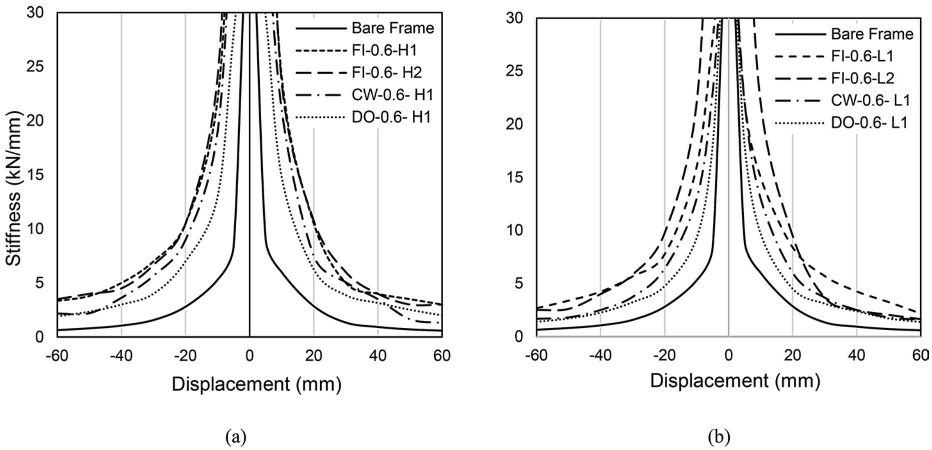

Fig. 9 Variation of stiffness versus displacement for specimens with different typologies for (**a**) high-strength infill and (**b**) low-strength infill

wall strength was lower for infill with opening, where 1.45 times greater capacity was found for the high-strength panel, and the maximum capacity of infill with opening was lesser by 1.4 times compared with full infill frame (Fig. 8(a)). Thick infill walls were found to have higher lateral capacity in comparison with thin infill by 1.3 to 1.57 times depending on the infill strength (Fig. 8(b)).

The lateral stiffness of the specimens is calculated as the ratio of the lateral load to the lateral displacement at each cycle and presented in Fig. 9. In all cases, the existence of infill increases the lateral stiffness in comparison with the bare frames. The stiffness ratio for strong infill panels was greater by an average of 2 times that of the corresponding weak infill. However, low-strength infills have shown better ductility behaviour in comparison with high-strength infills, where a noticeable reduction in ductility has been observed for high-strength infills under increasing displacement, especially for short infills. A lower reduction in ductility was observed for solid square infill and infill with openings. Specimens with openings showed lower stiffness in comparison with fully infill frames. The difference in stiffness in terms of wall thickness was insignificant for high-strength walls.

4.2 Damage state definition and assessment

Several studies have discussed the definition of the damage state of masonry infill walls (Cardone and Perrone 2015; Chiozzi and Miranda 2017; Liu et al. 2022). Some researchers have utilized the observation on the extent and severity of cracking patterns or failure typology of brick units as indicators for defining different DSs. In contrast, others have adopted the attainment of the peak load of the infilled frame or the achievement of given strength reduction. The definitions of DSs in literature as summarized by Xie et al. (2022) presented in Table 5.

The existing damage state definitions either focus solely on macroscopic damage without considering the mechanical properties of the infill wall or lack detailed descriptions of the damage phenomena rendering them less applicable in real earthquake scenarios (Liu et al. 2022). The skeleton curve characteristics do not strongly correlate with visual damage and should be avoided in fragility assessments (Xie et al. 2022). Besides, there are limited quantitative measurements about damage characteristics (e.g. crack width) in most experimental tests, making it difficult to establish reliable correlations between observed damage and existing DSs definition (Vintzileou et al. 2020; Liu et al. 2024). This highlights the need for more reliable damage assessment criteria to enhance the accuracy of damage evaluation.

Among the proposed DS definitions, this study relies on the maximum crack width criterion as a reference for evaluating the damage severity associated with each damage state, as it is quantitative, feasible, and more reliable than other methods (Xie et al. 2022). The damage state of the thirty-seven specimens developed herein has been evaluated based on the maximum crack width criteria presented in Table 6. Next, at each DS, the cumulative damage characteristics including cracks, crack width, and pattern have been recorded. The cracks with a width larger than 1 mm are considered visible, reflecting the visual crack detectability under inspection conditions (Korswagen et al. 2019). Hence, the percentage of wall area affected by clearly visible cracks is evaluated numerically using Eq. (2).

$$\text{Percentage of cracking} = \left(\frac{\text{Wall area effect by visible cracks}}{\text{Total wall area}}\right) \times 100 \tag{2}$$

Table 5 Damage state definition

DS	Phenomena-based criteria	Maximum crack width	Force-displacement skeleton curve
DS1	Initiation of cracks mainly in bed and head joints, with no significant brick crushing or joint sliding.	1 mm	2/3 peak strength
DS2	Significant diagonal cracks exceed 2 mm width spreading over masonry units and mortar joints with limited joints sliding and units crushing at corners.	2 mm	Peak strength
DS3	Development of wide diagonal cracks (usually larger than 4 mm) with widespread crushing and spalling of masonry units and significant joint sliding.	4 mm	20% strength loss

Table 6 Inter-storey drift values at the onset of damage States

No.	Specimens	N[a]	DS1 (%)	DS2 (%)	DS3 (%)	DS4 (%)
1	FI-0.6-L1	3	0.1–0.15	0.55–0.75	1.5–1.7	2.1–2.25
2	FI-0.6-L2	2	0.15	0.55–0.8	1.6–2	2.25–2.5
3	FI-0.6-H1	3	0.1–0.15	0.7–0.8	1.85–2.2	2.5–3
4	FI-0.6-H2	2	0.1–0.15	0.8	2–2.15	3
5	FI-1.0-L1	2	0.05–0.1	0.8–0.9	1.75–1.9	2.4–2.6
6	FI-1.0-L2	2	0.15	0.75–0.8	2.15–2.25	3–3.25
7	FI-1.0- H1	3	0.1	1–1.15	2–2.2	2.9–3.2
8	FI-1.0- H2	2	0.1	1.2	2.13	3.1
9	FI-1.6- L1	2	0.11– 0.15	0.74–0.81	1.41–1.55	2.22–2.4
10	FI-1.6- H1	3	0.11	0.81–1.18	1.85–2.22	2.59–3.15
11	CW-0.6- L1	1	0.1	0.4	0.9	1.4
12	CW-1.0- L1	1	0.05	0.4	1.23	1.9
13	CW-1.6- L1	1	0.07	0.59	1.29	1.85
14	CW-0.6- H1	1	0.05	0.5	1.55	2.15
15	CW-1.0- H1	1	0.05	0.55	1.75	2.5
16	CW-1.6- H1	1	0.07	0.81	1.59	2.22
17	SW-0.6- L1	1	0.05	0.3	0.8	1.1
18	SW-0.6- H1	1	0.1	0.4	1.4	1.9
19	DO-0.6- L1	1	0.05	0.4	0.8	1.55
20	DO-1.0- L1	1	0.05	0.4	2.5	2.15
21	DO-0.6- H1	1	0.1	0.4	1.5	2
22	DO-1.0- H1	1	0.05	0.5	1.55	2.5

a N = number of analyzed specimens

The observed results have shown noticeable effects of infill strength in terms of damage characteristics on both the wall and RC frame. Although there are similar observations about the influence of infill strength on accumulative damage have been highlighted in the literature (Sassun et al. 2016; Liu et al. 2024), its effects have yet to be characterized in the context of DS definition and fragility assessment. Therefore, new damage state criteria have been established, considering both the damage characteristics and the mechanical properties of infill walls. The suggested DS definition takes into account the damage status for both the infill wall and RC frame and can be assessed through visual inspection or available data in the literature, without requiring additional specific details on damage progression. The proposed criteria are categorized into four stages, DS1 to DS4.

- DS1: Minor cracks appear along with the initial detachment of the infill from the RC frame at the top of the wall. There is no damage observed in the RC frame, and the influence of infill properties remains insignificant.
- DS2: Low-strength masonry exhibits diagonal cracking with limited mortar joint sliding. Visible cracks are observed, covering approximately 10–20% of the panel area. In contrast, high-strength infills primarily show concentrated mortar joint sliding at the wall corners, with a lower crack intensity affecting less than 10% of the panel surface. Minor cracking also develops at the column ends.
- DS3: Low-strength masonry experiences extensive diagonal cracking and sliding, accompanied by brick unit crushing and spalling. Visible cracks cover 30–40% of the wall area, with cracks up to 2 mm at the column ends. High-strength infill exhibits mortar

sliding, along with individual diagonal cracks and localized brick failure at the corners. Cracks affect 10–25% of the wall area, with major cracks (width > 4 mm) at the column ends and the initiation of shear cracks in the columns.

- DS4: Low-strength masonry develops wide diagonal cracks with significant mortar sliding across the wall, leading to partial or total collapse. Visible cracks extend over more than 40% of the wall area, accompanied by crushing at the column ends. High-strength infill exhibits intensive mortar sliding at the corners, significant individual diagonal cracks, and crushing at the corners. Visible cracks spread over more than 25% of the panel area, with column-end crushing. Major shear cracks (up to 4 mm) have been also captured in the columns, along with the initiation of cracks in the middle of the top beam.

The proposed criteria categorize the damage progression for both the infill wall and RC frame, enabling assessment based on visual inspection or available data in the literature, without requiring additional details on crack width limits. The damage state definitions established in this study are summarized in Table 7. As shown, several specimens exhibited higher inter-story drift values, particularly DS2, DS3, and DS4, than those reported in the literature. This variation can be attributed to the scale of the specimens used, particularly the use of scaled frames with non-scaled brick. Although the size of the used bricks with respect to the specimen scale (2/3) was small enough to minimize scale effects, it may introduce artificial confinement effects, leading to an overestimation of lateral strength and displacement capacity. Similar observations have been noted in the literature, where higher inter-

Table 7 Proposed damage state (DS) criteria

Infill strength	DS	Masonry wall state	RC frame state
Low strength panel ($F_m \leq$ 6 MPa)	DS1	1–2 cracks in diagonal direction with first detachment of panel from RC frame.	No damage
	DS2	Cracks in diagonal direction corresponding to 20% of wall area with limited mortar sliding.	No visible cracks
	DS3	Intensive cracking and sliding along diagonal, with crushing and spalling of brick unit (30–40% of wall area affected by visible cracks).	Cracks at the column ends
	DS4	Wide diagonal cracks with significant mortar sliding separated over wall area, partial or total collapse expected. More than 40% effected by visible cracks.	Crushing at the column ends
High strength panel (F_m >6 MPa)	DS1	1–2 cracks in diagonal direction with initial detachment of panel from RC frame.	No damage
	DS2	Crack in diagonal direction with mortar sliding at a corner. Less than 10% of wall area influenced by visible cracks.	Minor cracks at column ends
	DS3	Sliding of mortar at corners with individual diagonal crack, failure of individual bricks at corners (10% to 25% of wall area impacted by visible cracks).	Major cracks at the column ends with the initiation of shear cracks in the mid-hight columns
	DS4	Intensive sliding at corners with significant diagonal cracks, crushing of corners. More than 25% of wall area is effected by visible cracks.	Crushing of column-end. Major shear cracks at the mid-hight of columns, along with cracks at the middle of the top beam.

story drift values are commonly associated with scaled specimens compared to full-scale specimens (De Risi et al. 2018; Liu et al. 2022, 2024). Additionally, these differences are also related to the combined effects of infill properties, boundary conditions, and damage state definitions. These factors should be considered when applying these findings in performance assessments and fragility analysis. The percentage of wall area impacted by visible cracks under increasing lateral load is shown in Fig. 10. Specimens presented in Fig. 10 were categorized based on infill strength, namely low ($F_m \leq 6$ MPa) and high ($F_m > 6$ MPa) strengths, where each colour refers to different specimens.

4.3 Damage phenomena for analysis samples

For low-bond strength short panels (FI-0.6-L1), slight diagonal cracks were initiated during the first two drift amplitudes of ISD = 0.15%. The maximum crack width exceeds 2 mm at ISD > 1%. Cracking and sliding are mainly concentrated along the wall diagonal and more intensively between the mid-height and top corners of the masonry panel. As ISD increased, significant sliding on the mortar was observed with the development of major diagonal cracks. Intensive cracking and sliding with major cracks at the column ends were developed at ISD > 1.5%. The damage became severe with significant mortar sliding as the lateral drift continued to increase. Better performance in terms of damage capacity was found for low-bond strength with AR between 1 and 1.6 (e.g. FI-1.0-L1). The maximum width of cracks reached 2 mm at ISD > 1.5%. Major cracks up to 3 mm at column ends with minor shear cracks were observed at relatively high drift (ISD > 3%). For this type of wall, shear sliding was the most common failure mode. Details of observed crack patterns are shown in Fig. 11(a). However, the infill with a very low brick strength of 2 MPa, which will be designated as FI-0.6-L1-LS for reference (Fig. 11(b)), showed lower mortar sliding and more extensive cracking on the bricks. The major cracks continued to grow with noticeable low mortar sliding as the story drift was increased. The ISD when crushing at the end of the columns was observed between 2.5% and 3%.

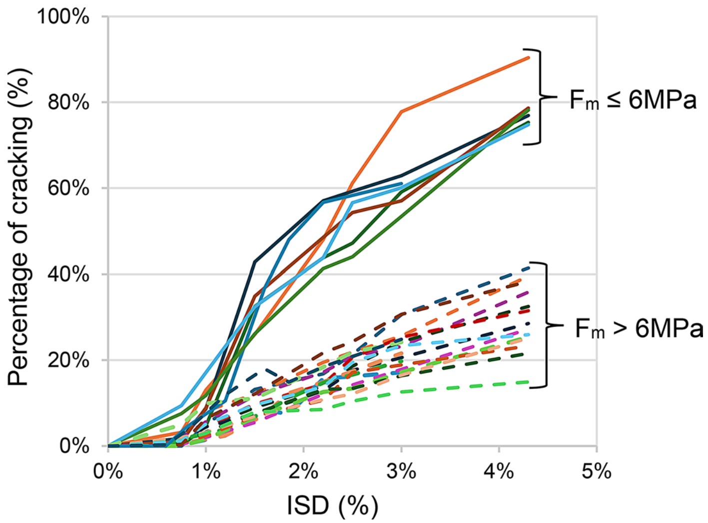

Fig. 10 The percentage of visible cracks for analysis models

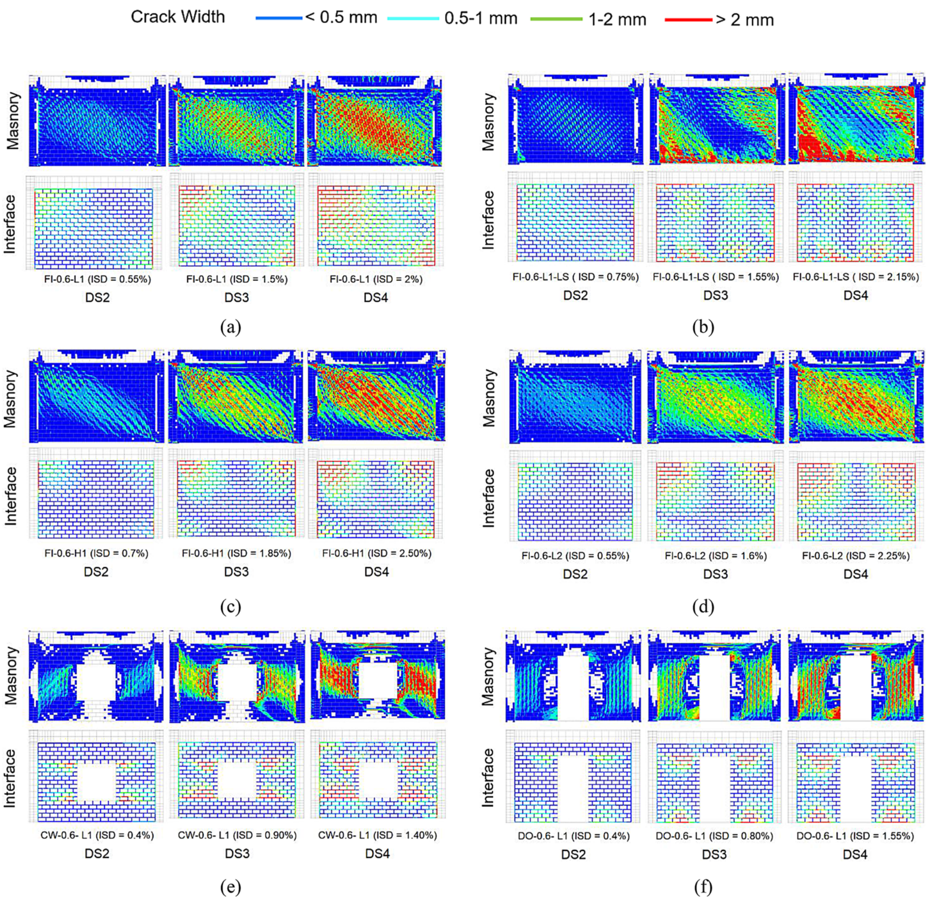

Fig. 11 Crack pattern on both masonry and interface of analysis models at DS2, DS3, and DS4 in panels with (**a**) FI-0.6-L1, (**b**) FI-0.6-L1-LS, (**c**) FI-0.6-H1, (**d**) FI-0.6-L2, (**e**) CW-0.6- L, and (**f**) DO-0.6- L1

For high-strength short panels (FI-0.6-H1), light cracks appear at the corners at a relatively low drift of 0.15% to 0.2% (Fig. 11(c)). Major cracks exceed 2 mm width observed at inter-story drift between 1.8% and 2%. Mortar sliding was significantly lower than the low-strength panel, where at a high drift level (ISD > 2%), mortar bed sliding was observed over 12% to 20% of the wall area. For this type of wall, damage was concentrated at the corners, where corner crushing was the dominant failure mode. Similar behaviour was captured for high-strength square and tall walls (AR between 1 and 1.6) in terms of crack pattern and failure mode, however, damage capacity was higher. Generally, lower sliding and cracking were developed for the square panel in comparison with the short wall at the same drift level.

Regardless of infill strength, an increase in wall thickness (ex: FI-0.6-L2) resulted in a noticeable reduction in the proportion of mortar failure, indicating that thicker walls are more resistant to mortar damage. At ISD < 2%, the number and width of cracks were not significantly different between 100 mm and 200 mm thickness infill wall. However, at a high drift level noticeable difference was captured (Fig. 11(d)).

For the infill with openings (e.g. CW-0.6- L1), the cracks initiated at the corners of the opening at ISD between 0.05% and 0.1% (Fig. 11(e) to (f)). Major cracks exceeding 2 mm in width developed at the sides of the opening before the drift reached 1%. Mortar bed sliding was separated over the wall portion between the opening and columns. The collapse area was observed in wall piers on the sides of the opening with the development of major cracks in columns ends at ISD > 2%. At higher drift levels (ISD > 3%), significant shear cracks were detected on columns with the total crush of column ends.

Overall, masonry properties have shown a noticeable effect on the damage behaviour of the infill RC frame. Short infill panels exhibited more severe damage relative to the applied drift, independent of other wall properties. In all cases, infill strength had a significant influence on the extent of damage, crack patterns, and failure modes.

More severe damage to the surrounding RC frame was captured with increasing infill strength. Moreover, the damage distribution and type of failure were extensively influenced by the relative strength between mortar and brick. Damage is concentrated at the lowest strength part of the panel namely mortar (low-bond strength (e.g. FI-0.6-L1)). A similar observation was found through validation models, where damage was mainly concentrated on brick units with minor joint sliding (MV1), while shear sliding of mortar joints was observed for low-bond strength specimens (MV 2 to 4). Results also showed a noticeable reduction in mortar sliding with increasing wall thickness, which has a direct impact on collapse behaviour and brick spalling as highlighted by Lu et al. (2020). The variation in the position of an opening (even when the percentage area of the opening remains constant) results in a change to the damage amount and failure mechanism, with the side window (SW) showing more intensive damage in comparison to the central window (CW). While doors, with the larger opening percentage in comparison with windows, showed insignificant differences in the number and width of cracks, which highlighted the influence of the type of opening on damage progress. Validation specimens with openings (MV3 to 4 and MV6 to 8) showed similar behaviour in terms of damage behaviour and failure mechanism.

The influence of the discussed parameters, particularly infill strength, thickness, and presence of opening, on damage behaviour of masonry infill is also aligned with the outlined drift limits in the draft of second-generation Eurocode 8 (prEN 1998-1-2:2025). The indicated inter-story drift limits, as specified in the code draft, showed a dependency on both the strength and thickness of the infill panel, where larger drift limits are specified for thicker and higher-strength masonry infill. In all cases, a reduction in drift limits for infills with openings was proposed, with a decrease of at least 20% compared to solid panels.

4.4 Drift base fragiy function

The ISD values related to the defined DSs were calculated for analysis samples. Based on the obtained data, the lognormal cumulative distribution fragility function (Fi) and the dispersion (βr) are evaluated according to Eqs (3) and (4) and listed in Table 8. βr accounts for both the specimen-to-specimen variability of the sample with different mechanical and geometric parameters. Fi is the standard normal (Gaussian) cumulative distribution function, θ is the median value of the probability distribution, βr is the logarithmic standard deviation, and N represents the total number of specimens tested.

Table 8 Parameters related to the proposed fragility functions for Hollow clay brick solid infill panels and distinction in terms of F_m

Description	N_{test}	DS1		DS2		DS3		DS4	
		ϴ	βr	ϴ	βr	ϴ	βr	ϴ	βr
All samples	23	-2.18	0.36	-0.18	0.33	0.62	0.29	0.97	0.29
$F_m \leq 6$ MPa	11	-2.14	0.42	-0.31	0.29	0.52	0.28	0.86	0.27
$F_m > 6$ MPa	12	-2.21	0.29	-0.07	0.32	0.72	0.26	1.07	0.26
AR − 0.6	9	-2.12	0.33	-0.34	0.29	0.59	0.28	0.90	0.28
AR − 1	9	-2.28	0.40	-0.07	0.3	0.68	0.27	1.02	0.27
AR − 1.6	5	-2.14	0.28	-0.08	0.33	0.58	0.31	0.97	0.28
Opening	12	-2.77	0.4	-0.78	0.36	0.26	0.38	0.64	0.35

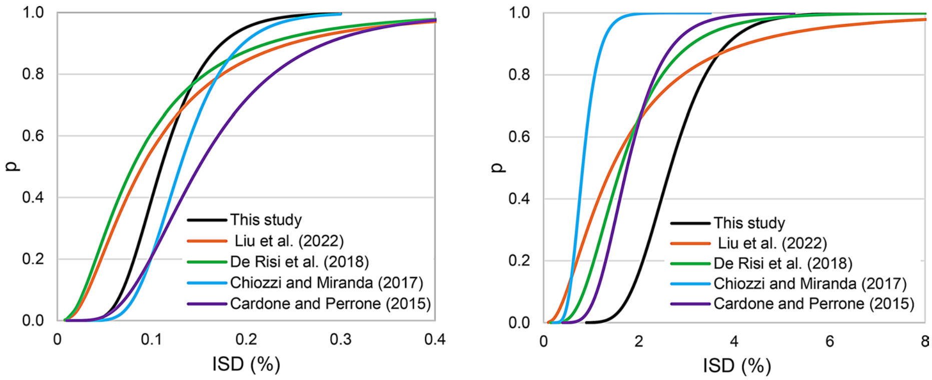

(a) (b)

Fig. 12 Comparison between evaluated fragility function in this study and literature at (**a**) initial damage state, and (**b**) collapse damage state

$$Fi\ (DS \geq\ ds|ISDj) =\ \Phi\left(\frac{Ln\ \left(\frac{ISD}{\theta}\right)}{\beta}\right) \tag{3}$$

$$\beta\ \mathrm{r} = \sqrt{\left(\frac{1}{\mathrm{N}-1}\sum\nolimits_{\mathrm{i}=1}^{\mathrm{N}}\left[\ln\left({}^{\mathrm{ISD}}/_{\theta}\right)\right]^2\right)^2} \tag{4}$$

A comprehensive collection of experimental results with various geometric and material properties was conducted in the literature to obtain the necessary data for developing fragility functions as explained in Sect. 1 (Chiozzi and Miranda 2017; Liu et al. 2022; and others). The average mean capacity measure at DS1 evaluated in this study was higher by 19% and 29% than the corresponding values reported by Liu et al. (2022) and De Risi et al. (2018) and lower by 10% and 28% in comparison with values founded by Chiozzi and Miranda (2017) and Cardone and Perroner (2015) respectively as shown in Fig. 12(a). The most significant differences were observed with values reported by Liu et al. (2022), where the values estimated herein were higher by 110%, 95%, and 60% respectively, while the lowest difference was found with those obtained by Cardone and Perrone (2015), lower than the values estimated in this study by 70%, 50%, and 40% respectively. The value calculated by De Risi et al. (2018) was smaller by 85%, 70%, and 48% in comparison with this study. Similarly, the reported by Chiozzi and Miranda (2017), with using of performance-based criteria, are lower by 87% and 75% respectively. These differences at the collapse stage are shown in Fig. 12(b).

Overall, these differences can be mainly justified based on (1) the difference in the type of data adopted, (2) lack of details about damage progress in literature, and (3) divergences in DS definitions. The specimens established herein were analyzed using the same frame type, loading protocol, and boundary conditions to ensure consistency in analysis and comparability of results. However, significant variations in data were found among the derived fragility functions by other studies, which may have a substantial effect on findings. For instance, Cardone and Perrone (2015) employ data including in-plane monotonic, cyclic, pseudo-dynamic load, and shaking table tests, while De Risi et al. (2018) considered only tests characterized by masonry infill with hollow clay bricks.

Most of the derived fragility function by other researchers mainly depended on the reported result by experimental studies in the literature. However, the provided description of the visible damage to the infill walls is very limited. To overcome this limitation, some researchers suggested the derivation of DSs based on the functional relationship between the ISD value related to a certain damage state and the ISD value corresponding to the peak load of the infill experimental response (De Risi et al. 2018; Liu et al. 2024). However, Xie et al. (2022) found that the characteristic points on the skeleton curves were not shown to strongly correlate with the extent of visual damage to the masonry walls and recommended to be avoided when developing fragility functions.

Moreover, the developed fragility function from the literature was based on different DS criteria, namely performance-based criteria and maximum crack width, among others. Xie et al. (2022) found significant variations between the derived fragility functions based on different DS definitions using the same experimental data.

In this study, the aforementioned challenges associated with the derivation of a high-quality fragility function namely data availability, damage description, and the large number of specimens requirement (FEMA – p58 recommended at least 5 specimens for developing of high-quality fragility function) were overcome using detailed numerical analysis.

The influence of masonry compressive strength on the definition of displacement thresholds corresponding to given physical damage levels has been also investigated (Fig. 13(a)). It was found that the average mean capacity measure of specimens characterized by F_m > 6 MPa was generally higher than ones with $F_m \leq 6$ MPa by 7% (DS1), 25% (DS2), 22%(DS3), and 24% (DS4). This finding partially confirms the trend reported by other studies, in which a significant influence of masonry infill compressive strength was observed for DS2 to DS4 as highlighted by De Risi et al. (2018) and for all DSs by Chiozzi and Miranda (2017). Nevertheless, a higher effect of infill strength was reported in the literature. These are mainly related to large variations in boundary conditions, type of frame, and wall dimensions from test to test, where the influence of these parameters has been neglected (Chiozzi and Miranda 2017).

The influence of the aspect ratio of the infill panel on displacement capacity was also investigated. Short infill walls showed lower displacement capacity in comparison with square or tall walls by about 5% (DS1), 26% (DS2), 10%(DS3), and 15% (DS4). The effect of wall thickness on given physical damage levels has been evaluated. Two subsets of sam-

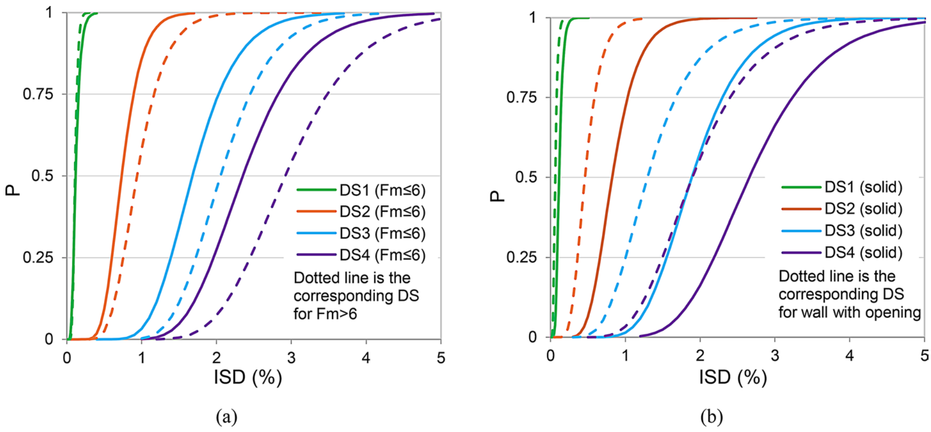

Fig. 13 Proposed fragility function based on (**a**) infill compressive strength, and (**b**) panel typology

ples with 100 mm and 200 mm infill thickness were considered. Through analysis, no significant differences in the in-plane damage state can be found. Nevertheless, the thick infill panel showed noticeably lower failure in mortar joints (interface), which may enhance the out-of-plane (OOP) capacity for masonry panels. The OOP capacity of the infill wall is not within the scope of this study.

The evaluation of the influence of openings in the damage assessment of masonry panels has been performed (Fig. 13(b)). Analysis results have found a significant effect of opening on displacement capacity for all damage states, with an average reduction of 55% for DS1 to DS2 and about 35% for DS3 and DS4 in comparison with full-infill walls. This comparison primarily focused on the effect of wall type on the damage probability by analyzing all full-infill walls against those with openings, with both groups containing walls that varied in key parameters such as infill strength and aspect ratio. The observed results were generally similar to the trend reported in the literature. In detail, Chiozzi and Miranda (2017) highlighted a significant reduction of masonry infill capacity for DS1 and DS2 in the presence of openings. De Risi et al. (2018) reported a 25% lower capacity for infill with openings at DS2, while a negligible influence was evaluated in terms of drift capacity at collapse. Finally, Cardone and Perrone (2015) suggested a reduction of about 25% in the presence of windows and of the order of 50% in the presence of doors for DS1 to DS3, and an equal drift capacity to panel without opening was assumed for DS4.

The calculated reduction for infill panels with opening by other research was based on quite a limited number of tests ignoring the variation in opening percentage, opening eccentricity, and the significant difference in the number of samples between solid infill and with opening. For instance, De Risi et al. (2018) evaluated only DS2 and DS4 because of insufficient details about damage progress and limited data. Moreover, the utilized data includes different opening percentages (between 10% and 40%) and opening eccentricity, which increase the divergences in findings.

5 Conclusions

In this study, in-plane drift-based fragility functions of masonry infill RC frame were derived based on micro finite element analysis. Numerous numerical models have been designed as a function of influential infill parameters including type of panel, strength, thickness, and aspect ratio. The total strain crack model and mohr-coulomb criterion have been adopted to describe the behaviour of masonry and interface respectively. Longitudinal and transversal steel reinforcements were modeled using of Menegotto-Pinto model. The displacement capacity at target damage states has been also calculated and compared with other studies. Findings were validated against experimental tests in the literature. The conclusions from this research are as follows:

- A damage state definition was introduced based on accumulative visible cracks under increasing lateral load considering both damage characteristics and the mechanical properties of walls. It can be assessed through visual inspection or available data in literature. The findings reveal that the damage states are directly related to ISD and infill strength.
- The determination of damage states is influenced by several parameters that introduce uncertainty. Infill strength emerged as the most influential parameter in determining in-plane drift ratios across moderate to collapse damage states. Higher probabilities of reaching damage states were associated with low-strength masonry. The presence of openings has a considerable impact on the fragility functions of all damage states. The aspect ratio exhibited a notable effect on the development of cracking at DS2, but its influence reduced as the damage progressed. The wall thickness showed an insignificant influence across the entire range of damage states.
- The damage behaviour of masonry infill subjected to in-plane load is affected by infill strength, type of panel, and aspect ratio. Infill strength significantly influenced the extent of damage and failure modes. The variation in the position of an opening alters the damage progression rate and affects the failure mechanism. Short infill walls exhibited the most intensive damage relative to the applied drift.
- The calculated in-plane drift values required to reach DS1, DS2, DS3, and DS4 were 0.11%, 0.84%, 1.86% and 2.64% respectively. The developed fragility functions were higher than those reported in the literature. The observed differences are directly related to the type of data, inadequate damage description, divergences in DS definitions, and possibly the use of scaled specimens.

This study advances the field of seismic vulnerability and risk evaluations by examining the impact of critical factors, including aspect ratio, infill strength, infill thickness, and the presence of openings, thereby providing a deeper understanding of the seismic behavior of masonry infill walls and their fragility assessment. Beyond the investigated parameters, future studies could explore the influence of scaling and type of loading on drift capacity to refine damage state calibration and strengthen the applicability of fragility functions. Future work should also focus on exploring the effect of in-plane damage on the out-of-plane capacity of infill walls, particularly regarding the reduced occurrence of mortar joint failure observed in thick walls.

Acknowledgements The authors would like to thank Universiti Putra Malaysia for the financial support of this research work under Geran Putra GP-IPS, GP-IPS/2023/9742800.

Author contributions Writing—original draft, SSK and NAB; Writing—review and editing, SSK, NAB, IAK, AHA and MZMT; Supervision, NAB, IAK, AHA and MZMT. All authors read and approved the final manuscript.

Funding Open access funding provided by The Ministry of Higher Education Malaysia and Universiti Putra Malaysia. This study was funded by Geran Putra GP-IPS, GP-IPS/2023/9742800.

Data availability The datasets generated and/or analyzed during the current study are available from the corresponding author on reasonable request.

Declarations

Conflict of interest The authors declare that they have no competing interests.

References

Al-Chaar G, Issa M, Sweeney S (2002) Behavior of masonry-infilled nonductile reinforced concrete frames. J Struct Eng 128(8):1055–1063. https://doi.org/10.1061/(ASCE)0733-9445(2002)128:8(1055)

Asteris PG, Antoniou ST, Sophianopoulos DS, Chrysostomou CZ (2011) Mathematical macromodeling of infilled frames: state of the Art. J Struct Eng 137:1508–1517. https://doi.org/10.1061/(ASCE)ST.1943-541X.0000384

ATC-24 (1992) Guidelines for Cyclic seismic testing of components of steel structures for buildings. Applied Technology Council, California

Baietti G (2021) Mode-I fracture parameters of quasi-brittle materials: direct evaluation using DIC and relationship with Mode-II interfacial parameters. Dissertation, University of Bologna

Banihashemi M, Wiebe L, Filiatrault A (2024) Suitable engineering demand parameters for acceleration-sensitive nonstructural components. Earthq Eng Struct Dynamics 53(14):4163–4182. https://doi.org/10.1002/eqe.4207

Basha SH, Kaushik HB (2016) Behavior and failure mechanisms of masonry-infilled RC frames (in low-rise buildings) subject to lateral loading. Eng Struct 111:233–245. https://doi.org/10.1016/j.engstruct.2015.12.034

Beyer K, Petry S, Tondelli M, Paparo A (2014) Towards displacement-based seismic design of modern unreinforced masonry structures. In: Ansal A (ed) Geotechnical, geological and earthquake engineering, vol 31. Springer, Cham, pp 401–428

Brooks JJ (2015) Concrete and masonry movements. Elsevier, Amsterdam

Butenweg C, Marinković M, Salatić R (2019) Experimental results of reinforced concrete frames with masonry infills under combined quasi-static in-plane and out-of-plane seismic loading. Bull Earthq Eng 17(7):3397–3422. https://doi.org/10.1007/s10518-019-00602-7

Calvi GM, Bolognini D (2001) Seismic response of reinforced concrete frames infilled with weakly reinforced masonry panels. J Earthquake Eng 5(2):153–185. https://doi.org/10.1080/13632460109350390

Cardone D, Perrone G (2015) Developing fragility curves and loss functions for masonry infill walls. Earthquakes Struct 9(1):257–279. https://doi.org/10.12989/eas.2015.9.1.257

Cavaleri L, Fossetti M, Papia M (2005) Infilled frames: developments in the evaluation of Cyclic behaviour under lateral loads. Struct Eng Mech 21(4):469–494. https://doi.org/10.12989/sem.2005.21.4.469

Chiozzi A, Miranda E (2017) Fragility functions for masonry infill walls with in-plane loading. Earthq Eng Struct Dynamics 46:2831–2850. https://doi.org/10.1002/eqe.2934

Combescure D, Pegon P (2000) Application of the local-to-global approach to the study of infilled frame structures under seismic loading. Nucl Eng Des 196(1):17–40. https://doi.org/10.1016/S0029-5493(99)00228-9

D'Altri AM, Messali F, Rots J et al (2019) A damaging block-based model for the analysis of the Cyclic behaviour of full-scale masonry structures. Eng Fract Mech 209:423–448. https://doi.org/10.1016/j.engfracmech.2018.11.046

Da Porto F, Guidi G, Dalla Benetta M, Verlato N (2013) Combined in-plane/out-of-plane experimental behaviour of reinforced and strengthened infill masonry walls. In 12th Canadian Masonry Symposium, Vancouver, Canada, pp 2–5

Decanini LD, Liberatore L, Mollaioli F (2014) Strength and stiffness reduction factors for infilled frames with openings. Earthq Eng Eng Vib 13(3):437–454

De Francesco F, Sullivan T, Nievas C (2022) Highlighting the need for multiple loading protocols in bi-directional testing. Bull New Z Soc Earthq Eng 55:80–94. https://doi.org/10.5459/bnzsee.55.2.80-94

Del Gaudio C, De Risi MT, Ricci P, Verderame GM (2019) Empirical drift-fragility functions and loss Estimation for infills in reinforced concrete frames under seismic loading. Bull Earthq Eng 17(3):1285–1330. https://doi.org/10.1007/s10518-018-0501-y

Demirel IO, Binici B, Yakut A (2023) In-plane seismic performance of different infill wall systems in ductile reinforced concrete frames. Bull Earthq Eng 21:3433–3459. https://doi.org/10.1007/s10518-023-01663-5

De Risi MT, Del Gaudio C, Ricci P, Verderame GM (2018) In-plane behaviour and damage assessment of masonry infills with Hollow clay bricks in RC frames. Eng Struct 168:257–275. https://doi.org/10.1016/j.engstruct.2018.04.065

De Villiers WI (2019) Computational and experimental modelling of masonry walling towards performance-based standardisation of alternative masonry units for low-income housing. Dissertation, Stellenbosch University

Dias-Oliveira J, Rodrigues H, Asteris PG, Varum H (2022) On the seismic behavior of masonry infilled frame structures. Buildings 12:1146. https://doi.org/10.3390/buildings12081146

Di Trapani F, Khan NA, Zhou L, Demartino C, Monti G (2024) Cyclic response of infilled RC frames with window and door openings: experimental results and damage interpretation. Earthq Eng Struct Dyn 53:43–67. https://doi.org/10.1002/eqe.4005

Drougkas A, Roca P, Molins C (2015) Compressive strength and elasticity of pure lime mortar masonry. Mater Struct 49:983–999. https://doi.org/10.1617/s11527-015-0553-2

Erdik M, Tümsa MBD, Pınar A et al (2023) A preliminary report on the February 6, 2023 earthquakes in Türkiye. Temblor. https://doi.org/10.32858/temblor.297

European Committee for Standardization (2005) Eurocode 8: design of structures for earthquake resistance – Part 3: assessment and retrofitting of buildings (EN 1998-3). CEN, Brussels

Federal Emergency Management Agency (2000) Prestandard and commentary for the seismic rehabilitation of buildings (FEMA 356). Federal Emergency Management Agency, Washington, DC

Federal Emergency Management Agency (2007) Interim testing protocols for determining the seismic performance characteristics of structural and nonstructural components (FEMA 461). Federal Emergency Management Agency, Washington, DC

Federal Emergency Management Agency (2018) Seismic performance assessment of buildings, volume 1 – methodology, second edition (Report No. FEMA P-58-1). Federal Emergency Management Agency, Washington, DC

Ferreira D (2021) DIANA FEA user's manual – Release 10.5. DIANA FEA BV. https://manuals.dianafea.com/d105/Home.html. Accessed 18 January 2025

Furtado A, De Risi MT (2020) Recent findings and open issues concerning the seismic behaviour of masonry infill walls in RC buildings. Adv Civil Eng 2020:9261716. https://doi.org/10.1155/2020/9261716

Furtado A, Rodrigues H, Arêde A, Varum H (2020) Experimental tests on strengthening strategies for masonry infill walls: A literature review. Constr Build Mater 263:120520. https://doi.org/10.1016/j.conbuildmat.2020.120520

Gaetani d'Aragona M, Polese M, Prota A (2024) Seismic fragility curves for infilled RC Building classes considering multiple sources of uncertainty. Eng Struct 321:118888. https://doi.org/10.1016/j.engstruct.2024.118888

Guadagnuolo M, Aurilio M, Faella G (2020) Retrofit assessment of masonry buildings through simplified structural analysis. Frattura Ed Integrità Strutturale 14:398–409. https://doi.org/10.3221/igf-esis.51.29

Hak S, Morandi P, Magenes G (2013) Evaluation of infill strut properties based on in-plane Cyclic tests. Građevinar 65(6):509–521. https://doi.org/10.14256/jce.868.2013

Hak S, Morandi P, Magenes G (2017) Prediction of inter-storey drifts for regular RC structures with masonry infills based on bare frame modelling. Bull Earthq Eng 16(2):397–425. https://doi.org/10.1007/s10518-017-0210-y

Huang Q, Guo Z, Zhu Y, Liu Y (2012) Experimental study on seismic behavior of RC frames infilled with concrete Hollow blocks. J Building Struct (Jianzhu Jiegou Xuebao) 33(2):110–118

Iannacone L, Andreini M, Gardoni P, Sassu M (2021) Probabilistic models and fragility estimates for unreinforced masonry walls subject to in-plane horizontal forces. J Struct Eng 147(4):04021039. https://doi.org/10.1061/(ASCE)ST.1943-541X.0003006

Kakaletsis DJ, Karayannis CG (2008) Influence of masonry strength and openings on infilled R/C frames under cycling loading. J Earthquake Eng 12:197–221. https://doi.org/10.1080/13632460701299138

Korswagen PA, Longo M, Meulman E, Rots JG (2019) Crack initiation and propagation in unreinforced masonry specimens subjected to repeated in-plane loading during light damage. Bull Earthq Eng 17:4651–4687. https://doi.org/10.1007/s10518-018-00553-5

Krawinkler H (2009) Loading histories for cyclic tests in support of performance assessment of structural components. In: 3rd International Conference on Advances in Experimental Structural Engineering, San Francisco, USA, October 2009

Kubalski T, Butenweg C, Marinković M, Klinkel S (2017) Investigation of the seismic behaviour of infill masonry using numerical modelling approaches. In 16th World Conference on Earthquake Engineering, Santiago, Chile

Liu C, Liu B, Wang X et al (2022) Seismic performance target and fragility of masonry infilled RC frames under in-plane loading. Buildings 12:1175. https://doi.org/10.3390/buildings12081175

Liu W, Jin W, Zhai C (2024) Fragility functions for masonry infill walls in RC frames with the in-plane and out-of-plane loading. J Building Eng 95:110177. https://doi.org/10.1016/j.jobe.2024.110177

Lu X, Yang Z, Chea C, Guan H (2020) Experimental study on earthquake-induced falling debris of exterior infill walls and its impact to pedestrian evacuation. Int J Disaster Risk Reduct 43:101372. https://doi.org/10.1016/j.ijdrr.2019.101372

Mehrabi AB, Shing PB, Schuller MP, Noland JL (1996) Experimental evaluation of masonry-infilled RC frames

Mergos PE, Beyer K (2014) Loading protocols for European regions of low to moderate seismicity. Bull Earthq Eng 12:2507–2530. https://doi.org/10.1007/s10518-014-9603-3

Milani G, Lourenço PB (2013) Simple homogenized model for the nonlinear analysis of FRP-strengthened masonry structures. II: Structural applications. J Eng Mech 139(1):77–93.

Ministry of Housing and Urban-Rural Development of the People's Republic of China (2016) Code for seismic design of buildings (GB 50011 – 2010). Architecture & Building, Beijing

Misir IS, Ozcelik O, Girgin SC, Yucel U (2016) The behavior of infill walls in RC frames under combined bidirectional loading. J Earthquake Eng 20(4):559–586. https://doi.org/10.1080/13632469.2015.1104748

Morandi P, Hak S, Magenes G (2018) Performance-based interpretation of in-plane Cyclic tests on RC frames with strong masonry infills. Eng Struct 156:503–521. https://doi.org/10.1016/j.engstruct.2017.11.058

Morandi P, Kurukulasuriya M, Milanesi RR, Bolognini D, Grottoli L, Dacarro F, Magenes G (2025) Dynamic shaking table out-of-plane tests on weak masonry infills with and without previous in-plane loading. J Building Eng 100:111670. https://doi.org/10.1016/j.jobe.2024.111670

Penava D, Anić F, Sarhosis V, Abrahamczyk L (2019) Distribution of shear resistance among components of RC frames with masonry infill walls containing confined door and window openings. In: Proceedings of the 7th International Conference on Computational Methods in Structural Dynamics and Earthquake Engineering (COMPDYN 2019), Crete, Greece, 24–26 June 2019. Eccomas Proceedia 1:2418–2430. https://doi.org/10.7712/120119.7084.18488

Penava D, Sigmund V, Kožar I (2016) Validation of a simplified micromodel for analysis of infilled RC frames exposed to Cyclic lateral loads. Bull Earthq Eng 14:2779–2804. https://doi.org/10.1007/s10518-016-9929-0

Prionas I, Mitchell J, Tan H (2020) Advanced FEA assessment of existing concrete floor diaphragms with low-ductility steel reinforcement. In: Proceedings of the 2020 New Zealand Society for Earthquake Engineering Annual Technical Conference, Christchurch, New Zealand, 22–24 April 2020

Sassun K, Sullivan TJ, Morandi P, Cardone D (2016) Characterising the in-plane seismic performance of infill masonry. Bull New Z Soc Earthq Eng 49:98–115. https://doi.org/10.5459/bnzsee.49.1.98-115

Shah SAA, Khan JS, Ali SM et al (2019) Shake table response of unreinforced masonry and reinforced concrete elements of special moment resisting frame. Adv Civil Eng 2019:7670813. https://doi.org/10.1155/2019/7670813

Sigmund V, Penava D (2012) Experimental study of masonry infilled R/C frames with opening. In: *15th World Conference on Earthquake Engineering*, Paper No. 2008, Lisbon, Portugal, pp 1–11. International Association for Earthquake Engineering

Stylianidis KC (2012) Experimental investigation of masonry infilled R/C frames. Open Constr Building Technol J 6:194–212. https://doi.org/10.2174/1874836801206010194

Van der Pluijm R, Rutten HS, Ceelen MACM (2000) Shear behaviour of bed joints. In: Proceedings of the 12th International Brick/Block Masonry Conference, Helsinki, Finland, 25–28 June 2000, pp 12

Verderame GM, Ricci P, De Risi MT, Del Gaudio C (2022) Experimental assessment and numerical modelling of conforming and non-conforming RC frames with and without infills. J Earthquake Eng 26:573–614. https://doi.org/10.1080/13632469.2019.1692098

Vintzileou E, Tselios I, Karagiannaki D (2020) Quantification of damage to masonry structures under seismic conditions. In: Kubica J, Kwiecień A, Bednarz Ł (eds) Brick and block masonry – From historical to sustainable masonry. CRC, London, pp 451–458. https://doi.org/10.1201/9781003098508-62

Xie X, Zhang L, Qu Z (2022) A critical review of methods for determining the damage States for the in-plane fragility of masonry infill walls. J Earthquake Eng 26(9):4523–4544. https://doi.org/10.1080/13632469.2020.1835749